Journal of Luminescence 248 (2022) 118809

Contents lists available at ScienceDirect

Journal of Luminescence

journal homepage: www.elsevier.com/locate/jlumin

# Influence of lanthanide (Gd, Tb or Ce) and silver doping on the luminescence lifetimes of calcium borate investigated by pulsed optically stimulated luminescence

Leonardo V.S. França [a,c,*], Fernanda H. Borges [b], Rogéria R. Gonçalves [b], Oswaldo Baffa [a], Eduardo G. Yukihara [c]

[a] Departamento de Física, FFCLRP, Universidade de São Paulo, Av. Bandeirantes, 3900, 14040-900, Ribeirão Preto, Brazil
[b] Departamento de Química, FFCLRP, Universidade de São Paulo, Av. Bandeirantes, 3900, 14040-900, Ribeirão Preto, Brazil
[c] Department of Radiation Safety and Security, Paul Scherrer Institute, Forschungsstrasse 111, 5232, Villigen PSI, Switzerland

ARTICLE INFO

*Keywords:*
Luminescence lifetimes
Calcium borate
Lanthanide doping
Silver doping
Pulsed optically stimulated luminescence
Time-tagged time-resolved data

ABSTRACT

The objective of this work is to evaluate the optically stimulated luminescence (OSL) lifetimes of different polycrystalline $CaB_6O_{10}$:Ln, $Ag_x$ (Ln = Gd, Tb and Ce; x: % molar concentration) compounds. For the determination of the luminescence lifetimes, time-tagged time-resolved (TTTR) data of the OSL under pulsed stimulation were analyzed. In addition, OSL emission spectra of the samples were recorded to correlate the emission bands with the estimated lifetimes. Whereas single Ce-doped compound presented a fast dominant component ($\tau < 0.41$ μs, ~63% of the signal), single Gd-doped compound exhibited a slow dominant component ($\tau = 2.3$ ms, ~67% of the signal). All Ag-codoped compounds (except for the Ce–Ag-codoped compound) presented a common dominant component with a ~43 μs lifetime, which is ascribed to a broad emission centered at ~330 nm. Both lifetimes and OSL emission spectra for the Gd-Ag-codoped compounds suggest that two luminescent centers compete for the radiative recombinations, confirming previous reported results. The relative Gd and Ag molar concentrations also had a strong influence in the estimated luminescence lifetimes of the slow component, probably due to the introduction of shallow trapping centers by silver doping. Furthermore, the temperature dependence of the common luminescence in Ag-codoped compounds appeared to be in agreement with the Mott-Seitz model for luminescence quenching. This work provides a better understanding of the physical processes and dynamics behind the radiative recombinations linked to OSL in borate compounds.

## 1. Introduction

Within the recombination processes responsible for the luminescence phenomenon, one of the physical parameters of main interest is the luminescence lifetime, which informs how fast the luminescence emission takes place after stimulation. The main factor governing the magnitude of the lifetime is the selection rules associated with the relaxation transition responsible for the emission of the luminescent center. Other factors such as the emission wavelength (for a given transition), temperature, luminescent center concentration and presence of shallow trapping centers may also influence the luminescence lifetimes [1–3]. In regard to the optically stimulated luminescence (OSL), which is the light emission of a previously irradiated material after light stimulation, two other factors may also influence the magnitude of the luminescence lifetime: the time needed to evict an electron from a trap and the time the electron takes to transition from the trap to the recombination center [4,5]. For a more in deep treatment on the principles of OSL lifetimes, one may consider the references hereinafter [4, 6–10].

One of the methods to determine the OSL lifetimes is based on time-tagged time-resolved (TTTR, or time-tagging) data of OSL under pulsed stimulation (POSL). POSL in general is a useful technique, since it allows for time-resolved discrimination of the decay components and the elimination of undesirable components. Consequently, a higher signal-to-noise ratio can be achieved compared to continuous wave OSL [7]. In a TTTR-POSL experiment, the samples are stimulated with light pulses and the detected photons are time-stamped with respect to the light pulses [7,11–14]. The data allows for the calculation of the

* Corresponding author. Departamento de Física, FFCLRP, Universidade de São Paulo, Av. Bandeirantes, 3900, 14040-900, Ribeirão Preto, Brazil.
*E-mail addresses:* leonardo.franca@psi.ch (L.V.S. França), eduardo.yukihara@psi.ch (E.G. Yukihara).

https://doi.org/10.1016/j.jlumin.2022.118809
Received 23 December 2021; Received in revised form 8 February 2022; Accepted 25 February 2022
Available online 11 March 2022

so-called photon arrival time distributions (PATDs), which is the distribution of detected photons as a function of arrival time since the beginning of the stimulation pulse [15]. From the PATDs, the lifetime components of the OSL signal following a stimulation pulse can be determined. More details about this approach and similar techniques can be found in previous reports [7,13,15,16].

Lifetime measurements not only can help to identify the luminescent centers present in a material, but can also reveal the presence of shallow trapping centers associated with thermoluminescence (TL) peaks below room temperature, having lifetimes in the order of microseconds to seconds at room temperature [7]. These shallow trapping centers may temporarily capture the released charges under optical stimulation, releasing them with a delay, which is characteristic of their trapping center lifetimes at room temperature. This effect may introduce additional lifetime components in the PATDs.

When analyzed at different temperatures, lifetime measurements can also be used to evaluate the thermal quenching of the luminescence, which is a decrease in luminescence efficiency with temperature. Considering the Mott-Seitz model of thermal quenching, in which the reduction in luminescence efficiency is caused by competing non-radiative relaxation routes whose probability increases with temperature [3], the temperature dependence of lifetime can be expressed as $\tau = \tau_0/(1 + \tau_0 \nu \exp(-E/kT))$, where $\nu$ and $E$ represent the frequency factor and activation energy (energy-gap between ground and excited states to have non-radiative processes preferable) of the luminescent center, respectively. Additional information about thermal quenching of luminescence can be found elsewhere [6,17,18].

Lanthanide-doping has proven to be useful for the development of luminescent materials for a wide-range of applications, including LEDs, lasers, scintillators, storage and X-ray phosphors applications [1,19–23]. This is due to the possibility of selecting wavelength emission and luminescence lifetimes, along with a relatively easy prediction of their energy levels in the host. OSL dosimetry has benefited from lanthanide doping as well. Several lanthanide-doped materials for OSL dosimetry applications can be found in the literature, including oxides, borates, aluminates, halides and sulphates [24–27]. In the case of OSL materials, it is important to determine whether the lanthanides act as recombination or as trapping centers, particularly in the presence of co-dopants [28].

Borate compounds typically present a defect created by oxygen vacancies, which act as electron trapping centers [29–31], as well as, a boron-oxygen hole center (BOHC), which is created by an oxygen that bridges a $BO_3$ and a $BO_4$ or two $BO_4$ groups [32–34]. These defects may have a special role on TL/OSL mechanisms of borate-based compounds.

In this context, a boron-based material, i.e., $CaB_6O_{10}$ (hereinafter referred to as CBO), has revealed some interesting properties. For instance, Ce, Li-codoped CBO was shown to have a wide linear dynamic range (2 mGy - 300 Gy) and two luminescence lifetimes of 70 ns and 143 ns, which are suitable for 2D dose mapping applications [35]. Lanthanide-doping in CBO structure is suitable since the ionic radius of the seven coordinated calcium ions (1.06 Å) is comparable to that of most $Ln^{3+}$ ions [36], which then facilitates incorporation by ion substitution in the lattice. In addition, the combination of Gd and Ag as dopants led to the development of a high sensitive OSL phosphor (minimum detectable dose = 40 μGy), with silver showing a special role on the luminescence enhancement of the phosphor [37]. Nevertheless, the role of lanthanide dopants in the TL/OSL of this material has not been systematically investigated. In particular, for further material development it would be helpful to understand the recombination processes in lanthanide-doped CBO and the influence of co-dopants.

The main objective of the present study is to evaluate the OSL lifetimes of lanthanide- (Gd, Ce or Tb) and silver-doped CBO compounds. Other Ln-doped CBO (Pr, Nd, Sm, Eu, Dy, Ho, Er, Tm and Yb) were previously investigated, but these compounds did not show significant OSL. Silver as dopant was demonstrated to enhance the luminescent response (intensity) of several phosphors, including that of Gd-doped CBO [37–39]. The use of different combination of dopants is desirable, since they may introduce new energy levels in the band gap of the host, including trapping and recombination centers, as well as incorporation of charge compensators in the crystal. A correlation of the luminescence lifetimes with the OSL emission bands is presented. Also this work provides insights into the role of silver on the luminescence of the phosphors involved. At last, the thermal quenching of the decay components associated with the main luminescence emission bands is presented, providing insights about the coupling between the luminescent centers and the surroundings in the lattice.

## 2. Materials and methods

### 2.1. Material synthesis

All polycrystalline compounds used in this work were synthesized by solid state reaction. This method consists of mixing proper amounts of starting precursors and then exposing the mixture to high temperatures. Calcium carbonate ($CaCO_3$) and boric acid ($H_3BO_3$) were the precursors used for the growth of the host compound. For the lanthanides and silver doping, suitable amounts of lanthanide and silver nitrates were added to the starting mixture. Then, the resultant compound was placed in a muffle furnace and the temperature was increased up to 800 °C, followed by a plateau for 3 h. Table 1 presents all chemicals used for the syntheses of doped CBO, as well as the molar concentrations of the dopants used. Specifically for the Gd-Ag-codoped compounds, three different combinations of molar concentrations were used, i.e., $Gd_{0.1\%}$-$Ag_{2\%}$, $Gd_{1\%}$-$Ag_{1\%}$ and $Gd_{2\%}$-$Ag_{0.2\%}$, represented in the text by Gd–Ag(1), Gd–Ag(2), Gd–Ag(3), respectively. It is worth mentioning that the percentages used for the dopants correspond to the relative amount of nitrate dopant used per amount of $CaCO_3$. A more detailed description of the synthesis procedure, including the amounts of the starting precursors used can be found in a previous work [37]. X-ray diffractograms for samples produced using the same method were also presented in this previous work. For the different combination of dopants used, with similar amounts of those reported here, the presented data showed that the expected phase for the CBO host was achieved.

### 2.2. OSL emission spectra acquisition

The OSL emission spectra were recorded with a Fluorolog 3 spectrofluorometer (FL3-22, Horiba Scientific) equipped with a double-grating monochromator at both excitation and emission positions. For excitation and light detection, a 450 W Xe lamp and a photomultiplier tube (R928, Hamamatsu) were used. For recording the spectra, the excitation was fixed at 430 nm and the detection range set between 270 and 400 nm. All entrance and exit slits of both excitation and detection was set as 5 nm. A longpass GG400 filter (Schott AG) was used on the excitation to avoid stimulation and detection of second-harmonic components. All spectra acquisitions were recorded using an increment of 1 nm per 0.1 s. Several sweeps had been carried out until the irradiation-induced signal was depleted significantly. All spectra were corrected by the detector system responsivity.

Prior to OSL measurements, the samples were irradiated using an Isovolt titan source model E−160 M2 (maximum energy and current of 160 kV and 10 mA, respectively) with a 0.8 mm beryllium window and a 2 mm aluminum filter. A dose of ~100 Gy was used to ensure a reasonable signal-to-noise ratio in the spectra. The dose reported here is air kerma measured using a calibrated ionization chamber.

### 2.3. TTTR-POSL readout

TTTR-POSL measurements were carried out using a Risø TL/OSL reader (TL/OSL-DA-20, DTU Nutech) equipped with a time counter board (TimeHarp 260 NANO, PicoQuant). The TimeHarp board with a 0.25 ns base resolution and a deadtime < 2 ns enables recording indi-

**Table 1**
Chemicals used in the syntheses of the samples. The codoped compounds are presented with a hyphen in between the dopants used. The Gd-Ag* represents the compounds with three different combinations of Gd and Ag molar concentrations: $Gd_{0.1\%}$-$Ag_{2\%}$, $Gd_{1\%}$-$Ag_{1\%}$ and $Gd_{2\%}$-$Ag_{0.2\%}$. The percentages used for the dopants correspond to the relative amount of dopant nitrate used per amount of $CaCO_3$.

| Precursors | | Compounds |
|---|---|---|
| Calcium carbonate ($CaCO_3$, ACS, 99.0% min., Sigma-Aldrich) | | All compounds |
| Boric acid ($H_3BO_3$, | BioReagent, 99.5%, Sigma-Aldrich)<br>ACS, 99.5%, Sigma-Aldrich) | $Gd_{1\%}$, $Tb_{1\%}$, $Ag_{0.1\%}$, Gd-Ag*<br>$Ce_{0.5\%}$, $Ce_{0.5\%}$-$Ag_{0.5\%}$, $Tb_{0.5\%}$-$Ag_{0.5\%}$ |
| Gadolinium nitrate ($Gd(NO_3)_3{\cdot}6H_2O$, 99.9%, Sigma-Aldrich) | | $Gd_{1\%}$, Gd-Ag* |
| Terbium nitrate ($Tb(NO_3)_3$ | ·$xH_2O$, 99.9%, Alfa-Aesar)<br>·$5H_2O$, 99.9%, Sigma-Aldrich) | $Tb_{1\%}$<br>$Tb_{0.5\%}$-$Ag_{0.5\%}$ |
| Cerium nitrate ($CeNO_3)_3{\cdot}6H_2O$, 99.9%, Alfa-Aesar) | | $Ce_{0.5\%}$, $Ce_{0.5\%}$-$Ag_{0.5\%}$ |
| Silver nitrate ($AgNO_3$, | 99.8%, Cennabras)<br>99.9999%, Sigma-Aldrich) | $Ag_{0.1\%}$, Gd-Ag*<br>$Ce_{0.5\%}$-$Ag_{0.5\%}$, $Tb_{0.5\%}$-$Ag_{0.5\%}$ |

vidual photon events on its 32,768 channels. Details about the integration of a photon counting system with the Risø reader and signal data acquisition can be found in a previous report [15].

For each compound, 5 mg of powder uniformly dispersed on steel cups was used. For stimulation of the samples, LEDs with peak wavelength at 470 nm and 72 mW/cm$^2$ irradiance (SMBB series, Ushio Europe B.V.) were used. As reported in a previous work, these LEDs present nominal rise and fall times of 133 ns and 474 ns, respectively, which restricts data acquisition to the microsecond timescale [16]. The luminescence was detected using a photomultiplier tube (9107QB, ET Enterprises) with two U-340 filters (2.5 mm and 5 mm thickness, Hoya) in front of it. In addition, a combination of the 5 mm thick U-340 with a 313 nm or a 330 nm narrow-band filters (both hard coated, OD 4.0, 10 nm FWHM, Edmund Optics) was used for some studies with a Gd-Ag-codoped compound.

Prior to TTTR-POSL measurements, the samples were irradiated with a $^{90}Sr/^{90}Y$ beta source (~37 mGy/s, calibrated in $^{60}Co$ air kerma using $Al_2O_3$:C thin detectors) attached to the Risø reader. Unless otherwise specified, a dose of ~37 mGy was used. During the sequence of measurements, all samples were heated up to 500 °C before irradiation to ensure depletion of previous trapped charges. For the study of the temperature dependence of the lifetimes, TTTR-POSL measurements were carried out at different temperatures (room temperature and 50 °C up to 150 °C, in 25 °C step). An additional preheating at 200 °C in the Risø reader was carried out in between the irradiation and the TTTR-POSL measurements to empty the shallow traps and prevent overlapping of the OSL with TL.

For all compounds, three pulse periods in the TTTR-POSL measurements were used, i.e., 100 μs, 1000 μs and 10000 μs, with a pulse width of 10% relative to the pulse period and bin widths of 0.512 μs, 4.096 μs and 32.768 μs, respectively. For the Ce-doped compounds, which presented a very fast decay component, the bin widths used were 0.128 μs, 1.024 μs and 16.384 μs, respectively. All TTTR-POSL measurements were carried out over 120 s and the PATDs were reconstructed by integrating the photon arrival times over the aforementioned period. For the study of the dependence of lifetimes with temperature, specific acquisition parameters were chosen, as reported on the captions of the corresponding figures.

### 2.4. PATDs analysis

PATDs were analyzed either individually or using a global fitting of the data for different pulse widths, with the lifetimes shared among different datasets. For the lifetime estimations, both rise and decay parts of the PATDs were taken into consideration, i.e., the recombination rates during the stimulation period (saturating exponential) and the recombination rates after the stimulation (exponential decay). The fitting was performed based on the equations described in a previous report [16], which allow for the presence of multiple non-interacting recombination centers; see also Chithambo [7]. The integral of both rise and decay parts corresponds to the total luminescence during the pulse period. For practical purposes, the two main parameters taken into account were the estimated lifetimes and the pre-exponential factors ($S_i$), which are proportional to the intensity of the PATD individual components [16].

The instrumental background (including LED related effects) was measured for all samples and different pulse widths. The most significant backgrounds were for the Gd- and Tb-doped compounds, which corresponded to 2.5% (1000 μs pulse width) and 3.9% (100 μs pulse width) of the overall signal, respectively. For the other compounds, that showed to be lower than 1%. Therefore, the instrumental background was neglected in all analyses performed. As a result, the constant luminescence which appears as an offset in some of the PATDs is mostly associated with luminescence components with lifetimes much longer than the timescales in consideration.

In the reported results, the number in parentheses following the lifetimes is the numerical value of standard uncertainty referred to the corresponding last digits of the quoted result [40]. The different lifetime components for each compound are assigned as $\tau_1$, $\tau_2$ and $\tau_3$, with the condition $\tau_1 < \tau_2 < \tau_3$. Only the most representative results are shown in the main text. The complementary data are presented in the Supplementary Materials.

## 3. Results

### 3.1. OSL emission spectra

In order to make a correlation with the luminescence lifetimes, the OSL emission spectra for the different compounds were previously collected. For singly-doped compounds, the OSL emission spectra provided clear results only for Gd- and Ag-doped samples. The Gd-doped compound exhibited a sharp emission centered at 311 nm (Fig. 1a), which is attributed to the $^6P_J \rightarrow {}^8S_{7/2}$ transitions of $Gd^{3+}$ centers [41]. The Ag-doped compound showed a broad emission at 295 nm (Fig. 1b), probably associated to $4d^9 5s \rightarrow 4d^{10}$ transitions of $Ag^+$ luminescent centers. This emission is similar to that of isolated $Ag^+$ ions in Ag-doped $SrB_4O_7$ [42].

For the other singly-doped compounds, the results were less conclusive. Ce-doped compound showed a strong phosphorescence after irradiation (room temperature emission followed by X-rays excitation, which takes place without light stimulation), with peaks at ~330 nm and ~360 nm likely due to 5d → 4f transitions of $Ce^{3+}$ centers (see Fig. S1). However, this emission could not be distinguished from the OSL emission. In addition, the OSL emission from Tb-doped compound could not be observed even using a higher prior dose (~500 Gy).

For the Gd-Ag-coped samples, the OSL emission spectra showed two distinct emissions: the sharp $Gd^{3+}$ emission and a broad emission centered at ~330 nm (Fig. 2). The ~330 nm-band intensity relative to the $Gd^{3+}$ emission decreased with the relative Gd/Ag increase in the

molar concentration, i.e. from sample Gd–Ag(1) to sample Gd–Ag(3) (Fig. 2a–c). The Tb–Ag-codoped compound also exhibited a broad and intense emission band centered at 330 nm (Fig. 3), similar to that one seen in the Gd-Ag-codoped compounds. These results suggest that the 330 nm emission is associated with Ag-doping, even though this emission is shifted compared to that observed in the single Ag-doped compound (295 nm). Although the reason for this shift is not clear, the luminescence lifetimes of these compounds suggest that the different emission bands are associated with the same luminescent center, as later presented in this report.

The OSL emission spectra of single Gd- and Ag-doped as well as of the Gd–Ag(3)-codoped compounds were previously reported [37]. In that work, however, the spectra were recorded with a different detection system at different conditions and were not corrected for the detector system responsivity, which may account for the differences in comparison with the present work results.

The OSL emission spectra for the Ce–Ag-codoped compound were recorded as well. However, as for the Ce-doped compound, the sample exhibited a strong phosphorescence (see Fig. S1), which could not be discriminated from the OSL. These results suggest that Ce-doping is responsible for the introduction of shallow trapping centers in the CBO host compound.

### 3.2. Luminescence lifetimes of singly-doped compounds

The PATDs from Gd-doped compound revealed two main components, with estimated lifetimes $\tau_1 = 4.3(2)$ μs (Fig. 4a) and $\tau_2 = 2.263$ (20) ms (Fig. 4b). The latter accounts for almost 67% of the total signal

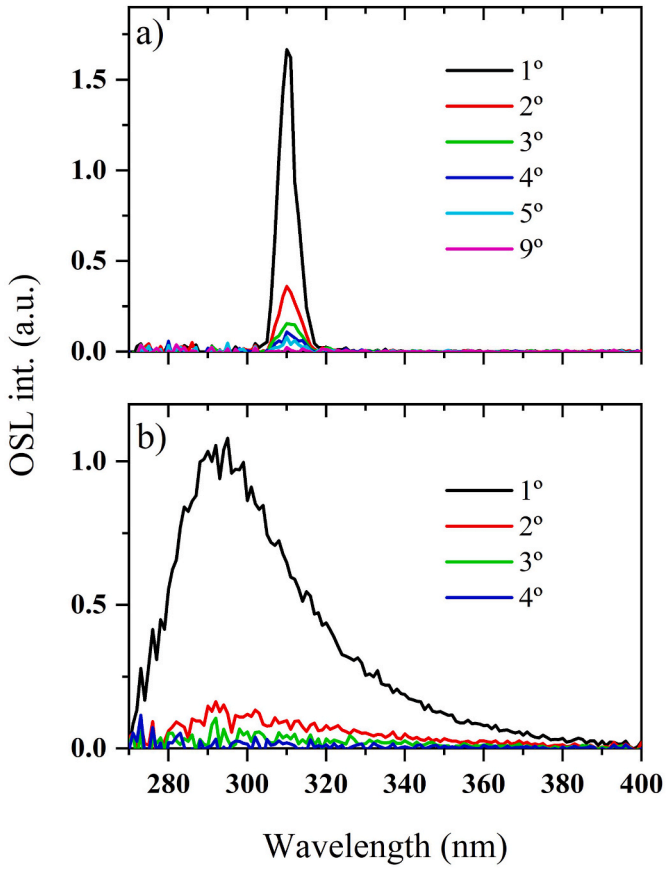


**Fig. 1.** OSL emission spectra of a) Gd- and b) Ag-doped compounds. Several spectra in a row were collected to show the depletion of the OSL, with the order indicated by the graph legends. Only the first spectra and the last one are shown. The spectra were background subtracted, considering the last acquisition as the background.

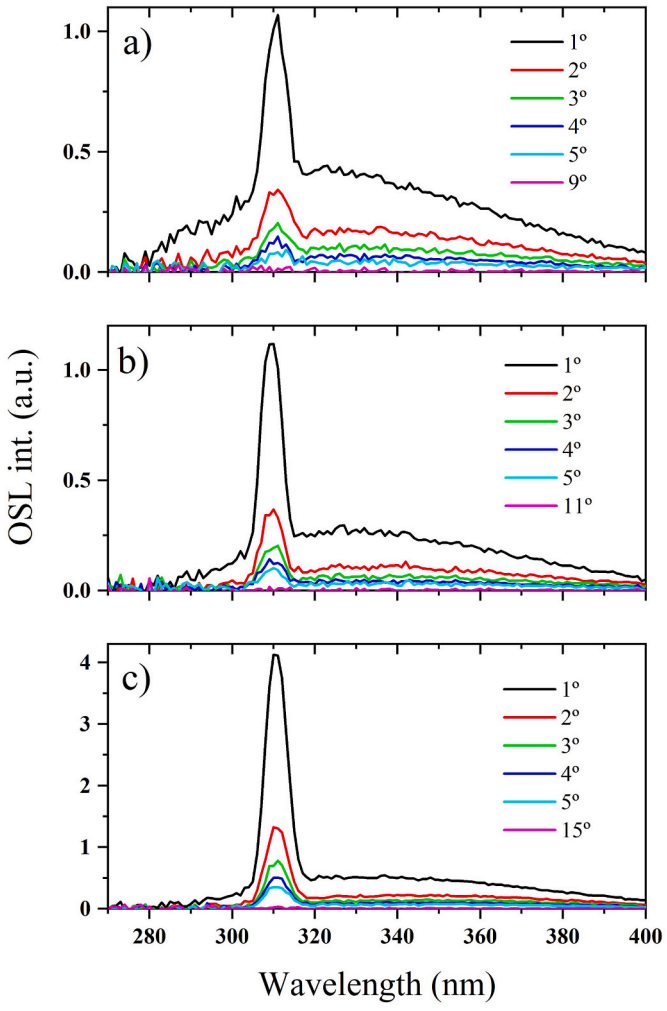


**Fig. 2.** OSL emission spectra for the Gd-Ag-codoped compounds. a) Gd–Ag(1); b) Gd–Ag(2) and c) Gd–Ag(3). The same acquisition parameters and corrections of the OSL emission spectra for the single-doped compounds apply.

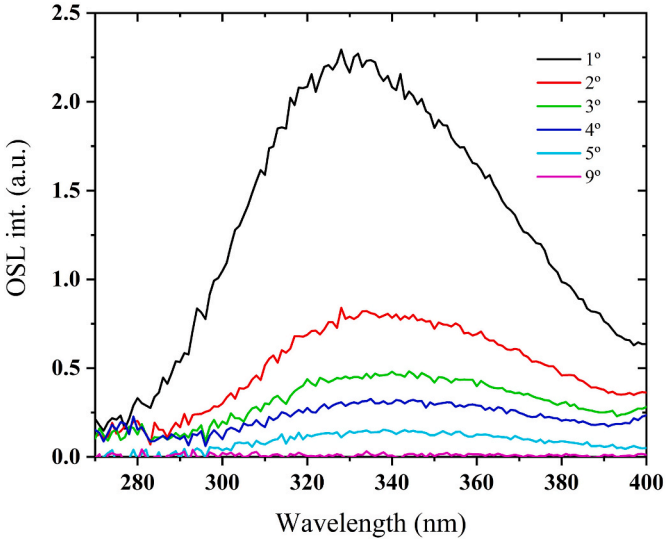


**Fig. 3.** OSL emission spectra for the Tb–Ag-codoped compound. The same acquisition parameters and corrections of the OSL emission spectra for the single-doped compounds apply.

(Fig. 4b). The ~2.3 ms lifetime is in agreement with the expected lifetimes for the forbidden transition $^6P_J \rightarrow {}^8S_{7/2}$ of $Gd^{3+}$, as reported for Gd-doped borate glasses [43,44] and, therefore, we attribute it to $Gd^{3+}$ centers. The analysis with the intermediate pulse width (100 μs) did not present additional components, but only showed the two components with either a poor resolution (fast component) or in a limited timescale (slow component) (see Fig. S2). The source of the fast component is unclear.

The Tb-doped compound exhibited two closely overlapped components with lifetimes of 4.1(1) μs and 40.1(30) μs (Fig. 5). Most of the signal, however, is due to a slow component, which appears as a constant component. Its lifetime could not be estimated even using a 1000 μs pulse width (Fig. S2). Given that the minor UV emission associated with $Tb^{3+}$ centers is typically associated with lifetimes of the order of 415–970 μs (for Tb molar concentration of 1%) [45,46], we attribute the lifetime components in the Tb-doped compound to unidentified luminescence centers. $Tb^{3+}$ emissions in the blue and green regions (main emission at 545 nm) of typical $Tb^{3+}$ centers are not considered here., since the detection window used in the measurements is restricted to the UV.

Ce-doped compound exhibited two components, with estimated lifetimes of $\tau_1 = 0.41(1)$ μs and $\tau_2 = 23(7)$ μs (Fig. 6), with the faster component contributing to 63.4% of the OSL signal. Typical lifetimes associated with 5d → 4f transitions of $Ce^{3+}$ are in the tens of nanosecond timescale, as reported for different compounds [47,48]. Considering that the lifetime of the $Ce^{3+}$ emission cannot be determined with the present equipment, the observed main lifetime is likely associated with the LED rise and fall times. Minor components with lifetimes ranging from 98 μs to 2.2 ms could also be observed (Fig. S2). These secondary components, including the 23 μs lifetime component, may be associated with shallow trapping centers, as suggested by the phosphorescence measurements. Nevertheless, the dominance of the $Ce^{3+}$ emission (faster component) is clearly demonstrated as seen in Fig. 6. Although the fast component lifetime could not be accurately estimated, this compound can be further investigated in view of 2D OSL dosimetry applications, since these require fast luminescent centers as $Ce^{3+}$ emission. Currently there is no commercial available OSL system for 2D dosimetry and recent attempts using $MgB_4O_7$-based films have shown some limitations, i.e., significant fading and OSL sensitivity changes [49].

The PATDs for the Ag-doped compound (Fig. 7) revealed components with lifetimes $\tau_1 = 5.0(2)$ μs and $\tau_2 = 38.9(9)$ μs, but these contributed only 6.5% ($\tau_1$) and 14.7% ($\tau_2$) to the overall signal (based on the 1000 μs pulse period, Fig. 7b), respectively. Most of the OSL is associated with a long luminescence lifetime component (78.8%) which appears as a constant in the PATDs. A component with a lifetime of $\tau_3 =$ 2.9(5) ms was also observed (Fig. 7c). This slow component as well as the dominant constant component are probably associated with shallow trapping centers introduced by Ag- doping. The TL curves (emission starting at 60 °C) of Ag-doped CBO reported in a previous work support this interpretation [37].

The ~39 μs component in Ag-doped compound is likely due to the presence of $Ag^+$ ions. $Ag^+$ luminescent centers in Ag-doped $SrB_4O_7$

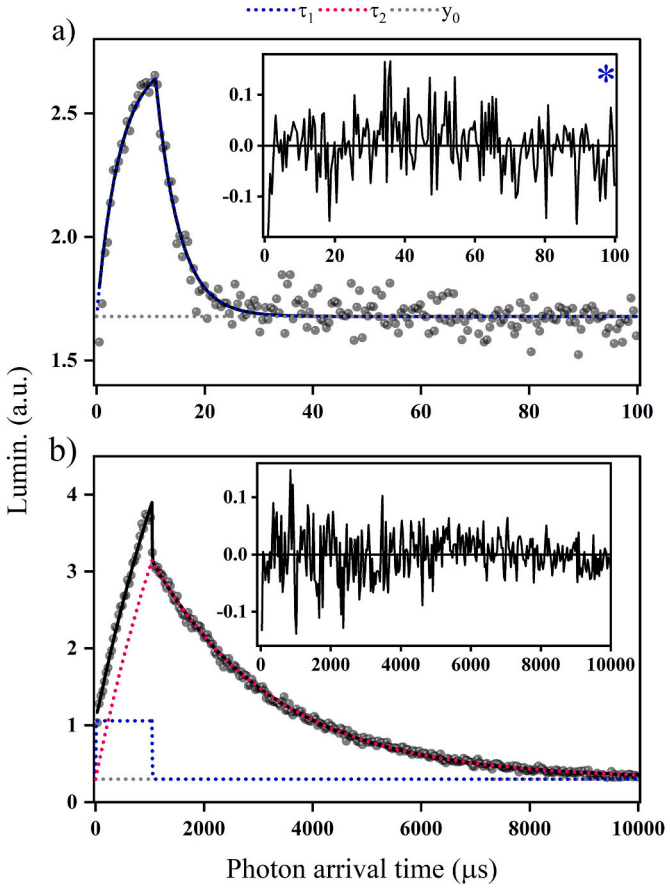


**Fig. 4.** PATDs fitting for the Gd-doped compound using two pulse widths: a) 10 μs and b) 1000 μs. When the 1000 μs pulse width was used, the fast component was forced to be that one found with the 10 μs pulse width. The insets show the residuals from the exponential fitting and the blue star indicates that the y-axis was adjusted for better visualization of the overall residuals. Both individual components are y-shifted for better comparison with the fitted curves (solid black lines).

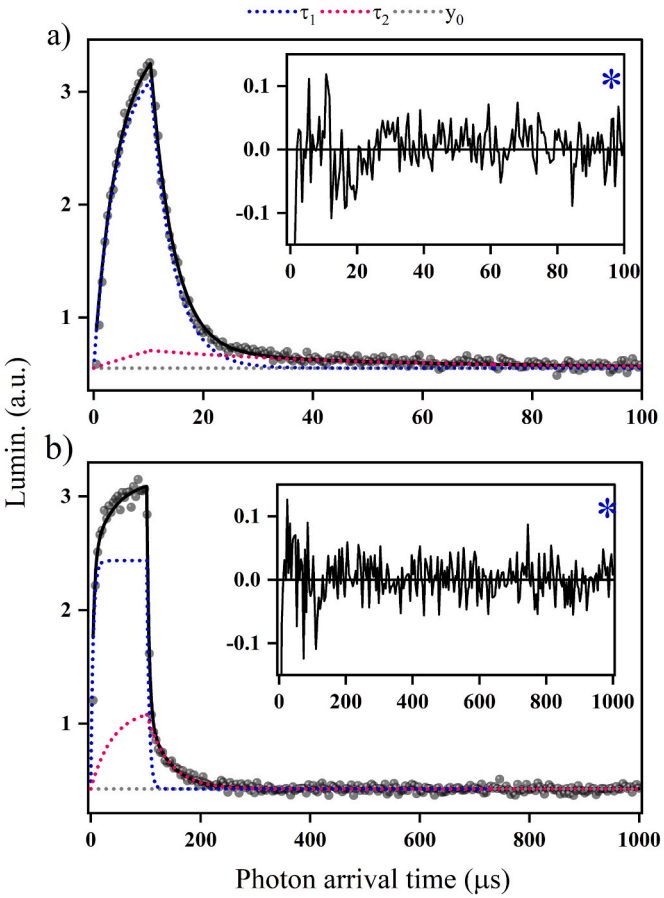


**Fig. 5.** PATDs fitting for the Tb-doped compound using two pulse widths: a) 10 μs and b) 100 μs. A biphasic exponential fitting was carried out with the lifetimes shared among the two pulse period datasets. For details about the insets and representation of the individual components, refer to the caption of Fig. 4. Dose used ~185 mGy.

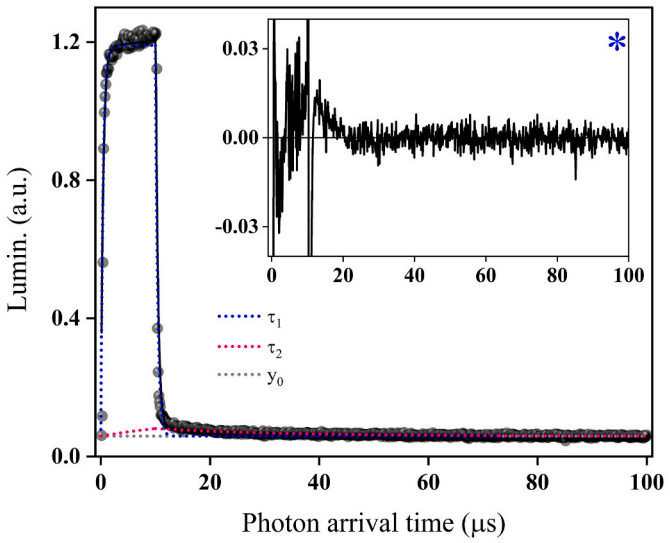


**Fig. 6.** PATD fitting for the Ce-doped compound when a 10 μs pulse width was used. For details about the insets and representation of the individual components, refer to the caption of Fig. 4. Dose used ~185 mGy.

crystals, which are responsible for a 290 nm emission, were found to be associated with an 11 μs lifetime [42]. Furthermore, $Ag^+$ ions in Ag-doped alkali halides were shown to be responsible for an emission with lifetime in the microsecond range, with a 34 μs lifetime at room temperature [50,51]. In Ag-doped aluminophosphate glasses, $Ag^+$ ions were also shown to be associated with decay components within the same timescale (1.3 μs and 11.7 μs lifetimes) [52]. The minor component with $\tau_1$ = 5.0 μs reported in the present work could not be identified.

### 3.3. Luminescence lifetimes of codoped compounds

The Gd-Ag-codoped compounds exhibited two main lifetime components, with $\tau_2$ varying between 41.0(3) μs and 44.6(2) μs and $\tau_3$ varying between 2.79(4) ms and 5.1(2) ms, depending on the relative Gd/Ag dopant concentration (Gd/Ag ratio increases from left to right, Fig. 8). $\tau_2$ values are similar to that of Ag-doped compound (39 μs), attributed to $Ag^+$ ions. Although $\tau_3$ of the Gd–Ag(3)-codoped compound (2.8 ms) is similar to the 2.3 ms component of the Gd-doped compound, $\tau_3$ of Gd–Ag(1)-codoped compound was considerably higher (5.1 ms, with substantial constant luminescence). This seems to be related to additional slower components as Ag amount increases, which can be caused by the introduction of shallow trapping centers. Energy transfer between the Gd and Ag ions is excluded, because $\tau_3$ decreases with the increase in the Gd/Ag concentration, when the opposite would be expected [43]. A faster component ($\tau_1$ ~1.8–6.1 μs lifetimes) was also observed, but its contribution to the PATDs compared to $\tau_2$ was negligible (Fig. S3).

A test was carried out to evaluate the reproducibility of the measured PATDs using different aliquots of the Gd–Ag(3)-codoped compound. The results from the three different aliquots did not present significant changes in the luminescence lifetimes or in their relative contributions to the PATDs. Excluding the constant component, the relative contribution to the PATDs for the fast and slow components were 56.1, 56.3, 57.4% and 43.9, 43.7, 42.6%, respectively (see Fig. S4).

For the Tb–Ag-doped compound, the PATDs showed a well defined component with a 42.8(7) μs lifetime (Fig. 9a), similar to the component in the Ag-doped and Gd-Ag-codoped compounds. This result supports the association of the ~43 μs component with the $Ag^+$ emission. Secondary components were also observed, but these components played a minor role compared to the 43 μs component (Fig. S5).

The Ce–Ag-codoped compound exhibited two main components, one with $\tau_1$ = 0.59(1) μs and another one with $\tau_2$ = 38.2(5) μs (Fig. 9b and c). By similarities with the singly-doped compounds, the faster component $\tau_1$ is probably due to $Ce^{3+}$ emission, whereas $\tau_2$ with the $Ag^+$ emission. As discussed for the Ce-doped sample, however, the estimated value of $\tau_1$ is likely associated with the LED rise and fall times. A component with a $\tau_3$ = 1.27(8) ms lifetime was also observed, but that was negligible compared to the other two (see Fig. S5).

Table 2 summarizes all the OSL emission band peaks as well as the estimated lifetimes along with their relative contribution (main components) to the PATDs for the compounds investigated. The table also shows the relative contribution of the constant components, which are probably associated with slower components.

### 3.4. Wavelength discrimination of the decay components for the Gd-Ag-codoped compound

The previous results suggest that, in CBO, the $Gd^{3+}$ emission (311 nm) is associated with a lifetime of ~2.8 ms, whereas the $Ag^+$ emission (~330 nm) is associated with a lifetime of ~43 μs. In order to confirm these identifications, PATDs for the Gd–Ag(3)-codoped compound were obtained using interference optical filters that transmit or block the $Gd^{3+}$ emission at 311 nm (IF313 or IF330, respectively). The broad emission band centered at ~330 nm, associated with $Ag^+$ centers, should be detected with both filters. The Gd–Ag(3) compound was

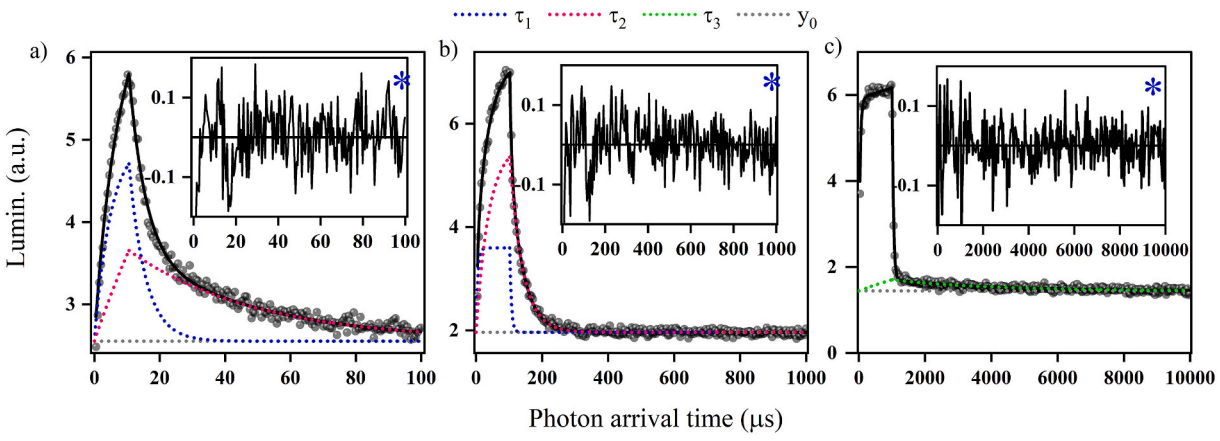


**Fig. 7.** PATDs fitting for the Ag-doped compound using three pulse widths: a) 10 μs; b) 100 μs and c) 1000 μs. A biphasic exponential fitting was carried out with the lifetimes shared among 100 μs and 1000 μs pulse period datasets. For the 10000 μs pulse period, a fitting was carried out individually and only the slower component is discriminated in the graph. For details about the insets and representation of the individual components, refer to the caption of Fig. 4. Dose used ~185 mGy.

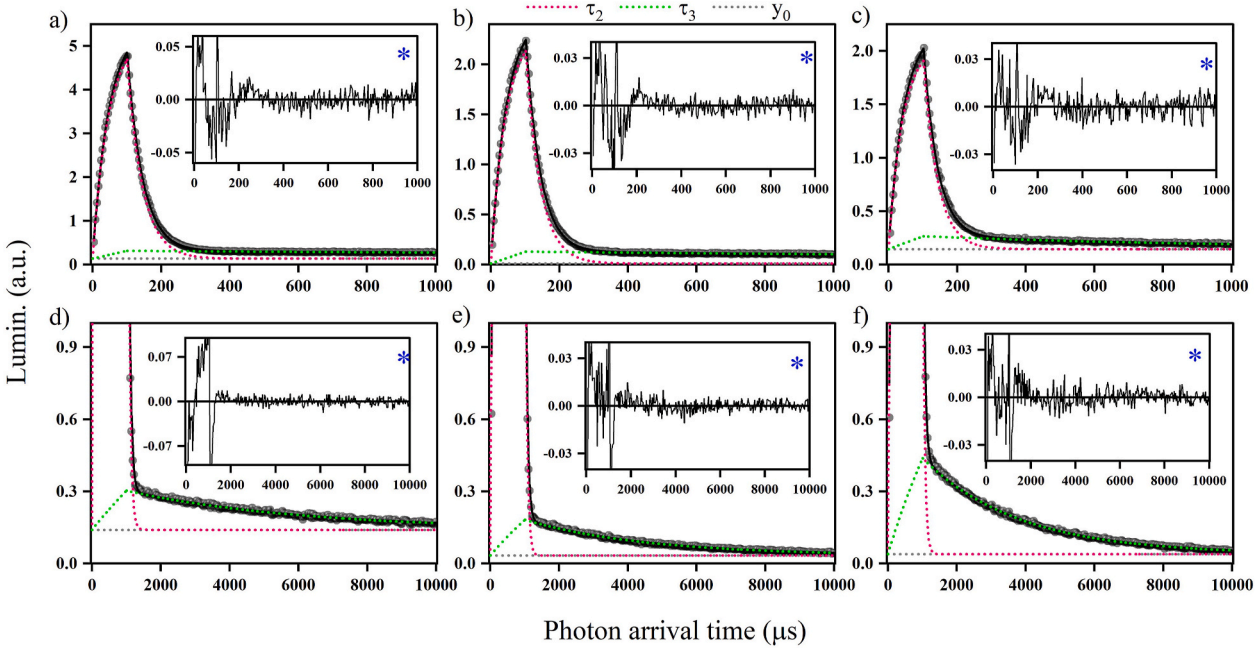


**Fig. 8.** PATDs fitting of the Gd-Ag-codoped compounds using two pulse widths (100 μs and 1000 μs). a) and d) Gd–Ag(1); b) and e) Gd–Ag(2); c) and f) Gd–Ag(3). For a better estimation of the lifetimes, a biphasic exponential fitting was carried out individually for each PATD. For details about the insets and representation of the individual components, refer to the caption of Fig. 4. For the 10000 μs pulse period, the y-axis was scaled up for better discrimination of the slower individual components.

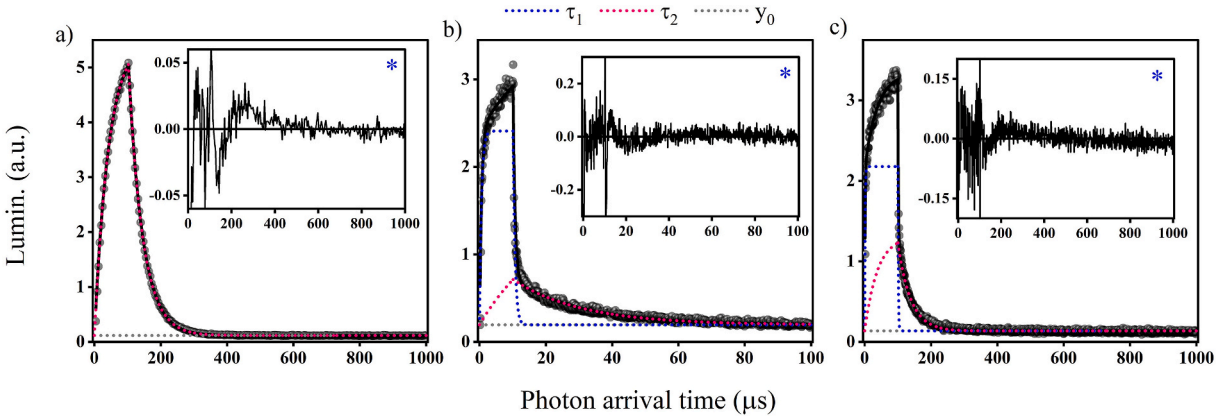


**Fig. 9.** PATDs fitting of two different samples: a) Tb–Ag-codoped compound using a 100 μs pulse width; b) and c) Ce–Ag-codoped compound using two different pulse widths (10 μs and 100 μs). The fitting for the Ce-doped compound was performed individually for each timescale. For details about the insets and representation of the individual components, refer to the caption of Fig. 4.

selected among the other Gd-Ag-codoped compounds since it showed to be less influenced by additional slower components (lifetime closer to that of Gd-doped compound - 2.3 ms).

As expected, using the IF330 filter (which blocks the $Gd^{3+}$ emission) the component with a millisecond lifetime is completely eliminated from the PATD (Fig. 10) and only a 43.1(4) μs lifetime component is observed. Conversely, using the IF313 filter (which transmits the $Gd^{3+}$ emission and blocks part of the $Ag^{+}$ emission) the main PATD main component presented a lifetime of 2.651(28) ms. Therefore, these results confirm the original identifications.

### 3.5. Luminescence lifetimes as a function of temperature

The luminescence thermal quenching of the compounds was investigated for Gd- and Tb-doped, as well as for Gd-Ag- and Tb–Ag-codoped compounds considering both lifetimes and integrals under the PATDs. For the Ce-doped compounds, these measurements were not performed, since the main component lifetime could not be estimated at room temperature.

For the Gd-doped compound, the 2.3 ms component corresponds to $^{6}P_{J} \rightarrow {}^{8}S_{7/2}$ forbidden transitions of $Gd^{3+}$ and, therefore, thermal quenching is expected to be negligible (weak coupling between ground and excited states). Indeed, the experimental lifetimes at room temperature and 150 °C were the same, but an anomalous increase was observed at intermediate temperatures (Fig. 11). This effect is probably caused by the influence of shallow trapping centers, as observed with $Al_2O_3$:C samples [3]. The overall luminescence (PATD area) decreased less than 10% over the same temperature range. For the Tb-doped compound, thermal quenching of the main decay component was analyzed as well. Although the origin of this component could not be elucidated, the results exhibited a strong thermal quenching over the temperature range analyzed (Fig. S6).

**Table 2**
OSL emissions and the estimated lifetimes for each combination of dopants. Unless specified by the footnotes, each lifetime was estimated considering a biphasic exponential fitting and based on different pulse widths: $\tau_1$ (10 μs), $\tau_2$ (100 μs) and $\tau_3$ (1000 μs). The relative contributions ($R_i$) to the PATDs were calculated by using the estimated lifetimes and the pre-exponential factors ($S_i$) for a specific pulse width (for italic and bold $R_i$, the pulse widths used were 10 and 100 μs, respectively. For the others, a 1000 μs pulse width was used). $R_{y_0}$ corresponds to the relative contribution from the constant component ($y_0$). For the Gd-Ag- and Tb–Ag-codoped compounds, the minor contribution from the fast components (see Supplementary Materials) was not taken into account.

| Dopants | OSL emissions (nm) | Lifetimes (μs) | | | | | | |
|---|---|---|---|---|---|---|---|---|
| | | $\tau_1$ | $R_1$ | $\tau_2$ | $R_2$ | $\tau_3$(x10$^3$) | $R_3$ | $R_{y_0}$ |
| Gd | 310 | 4.3(2)[a] | 6.7% | 2263(20)[b] | 66.9% | – | – | 26.4% |
| Tb | – | 4.1(1)[c] | **28.8%** | 40.1(30)[c] | **10.2%** | – | – | **61.1%** |
| Ce | – | <0.41(1) | *63.4%* | 23.5(69) | *3.5%* | 2.2(2)[d] | – | *33.1%* |
| Ag | 295 | 5.0(2)[c] | **6.5%** | 38.9(9)[c] | **14.7%** | 2.9(5) | – | **78.8%** |
| Gd–Ag(1) | 311, 325 | 1.8(1) | – | 44.6(2) | 65.9% | 5.1(2) | 12.1% | 22.0% |
| Gd–Ag(2) | 311, 330 | 4(1) | – | 42.5(2) | 67.7% | 3.6(2) | 20.4% | 11.9% |
| Gd–Ag(3) | 311, 340 | 6.1(8) | – | 41.0(3) | 48.5% | 2.79(4) | 39.4% | 12.1% |
| Tb–Ag | 332 | 4.0(7) | – | 42.8(2)[a] | 83.7% | 30(9) | 16.3% | – |
| Ce–Ag | – | <0.59(1) | **60.8%** | 38.2(5) | **35.1%** | 1.27(8) | – | **4.1%** |

[a] Lifetime estimation using a single component.
[b] Lifetime estimation using a 1000 μs pulse width.
[c] Lifetime estimation using a global fitting among two datasets (10 and 100 μs pulse widths).
[d] Lifetime estimation of the slower component in a three-component exponential fitting.

Thermal quenching for the luminescence of Ag-codoped compounds was also investigated. That was performed focusing on the common ~43 μs lifetime component of Gd-Ag- and Tb–Ag-codoped compounds. All samples presented similar behavior with significant thermal quenching in the temperature range analyzed (Fig. 12). That suggests that the common luminescent center characterized by a 43 μs lifetime is strongly affected by the lattice. The different combinations of dopants do not seem to have a significant influence on the thermal quenching of the common luminescence, which followed the equation for the Mott-Seitz model with similar fitting parameters. In addition, Fig. S7 shows the thermal quenching considering the overall luminescence, which showed to be in a good agreement with the temperature dependence of the lifetimes for the Ag-codoped compounds. $Ag^+$ emission is known to have strong thermal quenching up to room temperature [42,50]. Even though the temperature range used in the present study is higher compared to that of the reported works, the significant thermal quenching of $Ag^+$ emission is supported.

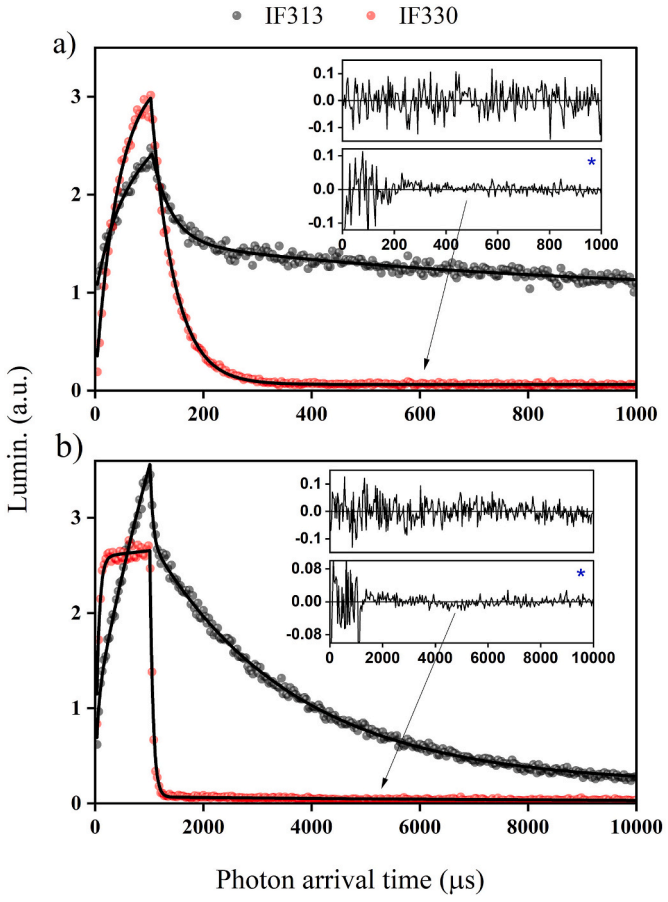


**Fig. 10.** PATDs for the Gd–Ag(3)-codoped compound collected with the narrow-band filters (IF313 and IF330) with two different pulse widths: a) 100 μs and b) 1000 μs. The insets correspond to the fitting residuals of the PATDs obtained with the different filters.

## 4. Conclusions

The results support the association of the 311 nm emission characteristic of $Gd^{3+}$ centers and the ~2.3 ms luminescence lifetime in the Gd-doped compounds. The negligible thermal quenching confirms the weak coupling between ground and excited states. The narrow emission and long luminescence lifetimes make Gd-doped compounds of interest for dosimetry applications, because the $Gd^{3+}$ emission can be easily isolated

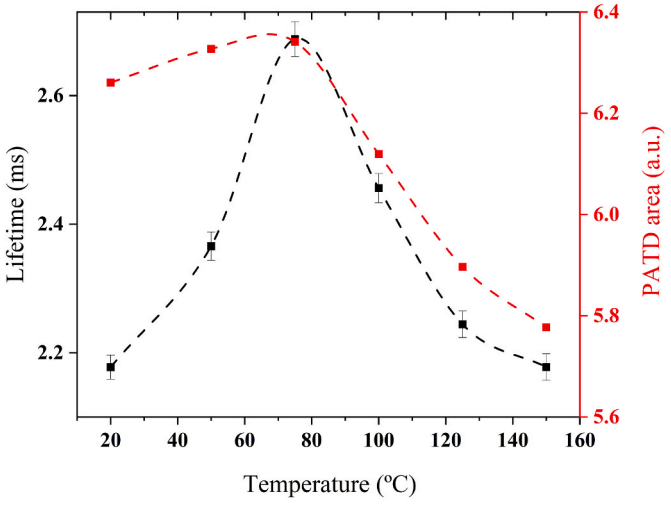


**Fig. 11.** Lifetimes and PATDs as a function of temperature for the Gd-doped compound. The lifetimes were obtained using a single-component exponential fitting for each temperature and the error bars represent their uncertainties. The PATDs are expressed as the integral under the fitted curves. The data was recorded using a 10000 μs pulse period (pulse width: 1000 μs). To export the data, a 32.768 μs bin width was used.

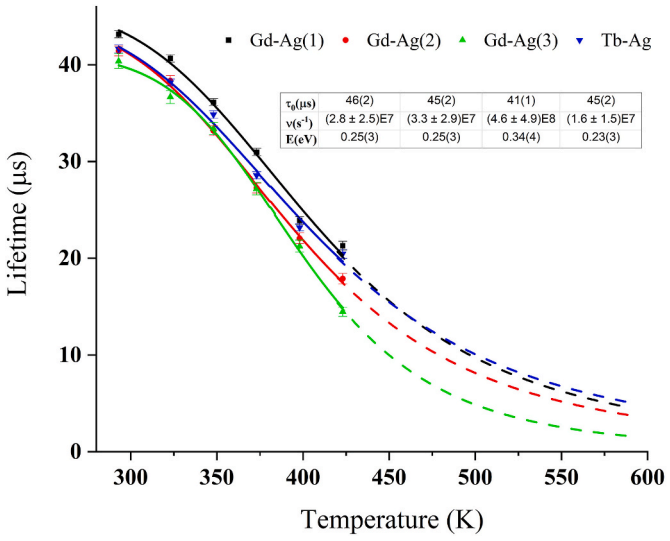


**Fig. 12.** Dependence of lifetimes on temperature for Gd-Ag- and Tb–Ag-codoped compounds in a single graph. The lifetimes correspond to that one of the dominant component of a biphasic exponential fitting. The error bars are the uncertainties related to the estimated lifetimes. The solid lines represent the fitted curves according to the equation $\tau = \tau_0/(1 + \tau_0\nu \exp(-E/kT))$, where $\nu$ and $E$ represent the frequency factor and activation energy, respectively. The dashed lines are the extrapolation for higher temperatures. The parameters in the table from left to right correspond to the legends in the same order. All data were recorded using a 400 μs pulse period (pulse width: 100 μs). To export the data, a 4.096 μs bin width was used.

either using optical filters or time-resolved measurements (e.g. POSL).

Ce-doping successfully introduced a fast component with lifetime faster than the LED rise and fall times (< 500 ns), but the simultaneous introduction of shallow trapping centers and a resultant strong phosphorescence did not allow for the OSL emission spectra to be collected. Nevertheless the OSL lifetime is consistent with $Ce^{3+}$ emission. Materials with fast luminescence lifetimes such as Ce-doped CBO can be useful in laser-scanning imaging for 2D OSL dosimetry. Nevertheless, one must investigate a new synthesis method or introduce a codopant that could lead to a more stable trapping center while minimizing the role of shallow trapping centers.

For the Ag-doped compounds, a broad emission centered at 295 nm in singly-doped compounds and at ~330 nm in co-doped compounds, associated with a lifetime in the 39–45 μs range, was observed, which is probably associated with $Ag^+$ ions. The wavelength difference between these bands may be related to the influence of the host or other defects introduced by co-doping on the $Ag^+$ emission. The thermal quenching of the 43 μs lifetime component in the Ag-codoped compounds supports this interpretation, showing a strong influence of the lattice in the luminescent emission. The lifetime of the Ag-doped samples is intermediate between that of Ce- and Gd-doped samples, being of potential interest for both laser-scanning imaging and applications using POSL. In addition, $Ag^+$ seems to compete with other recombination centers (e.g. $Gd^{3+}$ or $Ce^{3+}$). Therefore, Ag-codoping seems to improve the luminescence in CBO by providing an additional recombination route.

Although the exact lifetime estimations can be influenced by factors such as the relative intensity of the emission bands and the presence of shallow trapping centers, the results demonstrate the value of TTTR-POSL measurements combined with a systematic study of doped and co-doped compounds, which gives insights about the recombination mechanisms in OSL materials. The information on CBO presented here should be useful for future developments of this material.

## Credit author statement

**Leonardo V. S. França**: Conceptualization, Methodology, Investigation, Data curation, Writing – original draft, Visualization. **Fernanda H. Borges**: Data curation. **Rogéria R. Gonçalves**: Writing – review & editing. **Oswaldo Baffa**: Supervision, Writing – review & editing, Funding acquisition. **Eduardo G. Yukihara**: Conceptualization, Methodology, Supervision, Writing – review & editing, Funding acquisition.

## Declaration of competing interest

The authors declare that they have no known competing financial interests or personal relationships that could have appeared to influence the work reported in this paper.

## Aknowledgments

This research was partially funded by Brazilian agencies Fundação de Amparo à Pesquisa do Estado de São Paulo (FAPESP CEPID-NEUROMAT 13/07699-0), Coordenação de Aperfeiçoamento de Pessoal de Nível Superior (CAPES, Finance Code 001) and Conselho Nacional de Desenvolvimento Científico e Tecnológico (CNPq Grant 304107/2019-0). We are grateful to Eldereis de Paula for the technical support regarding the irradiation of samples. The Risø TL/OSL-DA-20 reader (DTU Nutech) was acquired with partial support from the Swiss National Science Foundation (R'Equip project 206021_177028).

## Appendix A. Supplementary data

Supplementary data to this article can be found online at https://doi.org/10.1016/j.jlumin.2022.118809.

## References

[1] G. Blasse, B.C. Grabmaier, Luminescent Materials, Springer-Verlag, 1994.
[2] H. Qin, D. Wu, J. Sathian, X. Xie, M. Ryan, F. Xie, Tuning the upconversion photoluminescence lifetimes of $NaYF_4$:$Yb^{3+}$, $Er^{3+}$ through lanthanide $Gd^{3+}$ doping, Sci. Rep. 8 (12683) (2018).
[3] M.S. Akselrod, N. Agersnap Larsen, V. Whitley, S.W.S. McKeever, Thermal quenching of F-center luminescence in $Al_2O_3$:C, J. Appl. Phys. 84 (6) (1998) 3364–3373.
[4] R.J. Clark, I.K. Bailiff, M.J. Tooley, A preliminary study of time-resolved luminescence in some feldspars, Radiat. Meas. 27 (2) (1997) 211–220.
[5] M.L. Chithambo, R.B. Galloway, On the slow component of luminescence stimulated from quartz by pulsed blue light-emitting diodes, Nucl. Instrum. Methods Phys. Res. B 183 (3) (2001) 358–368.
[6] E.G. Yukihara, S.W.S. McKeever, Optically Stimulated Luminescence: Fundamentals and Applications, Wiley, 2011.
[7] M.L. Chithambo, An Introduction to Time-Resolved Optically Stimulated Luminescence, Morgan and Claypool Publishers, 2018.
[8] I.K. Bailiff, Characteristics of time-resolved luminescence in quartz, Radiat. Meas. 32 (5) (2000) 401–405.
[9] M.L. Chithambo, The analysis of time-resolved optically stimulated luminescence: I. Theoretical considerations, J. Phys. Appl. Phys. 40 (7) (2007) 1874–1879.
[10] M.L. Chithambo, The analysis of time-resolved optically stimulated luminescence: II. Computer simulations and experimental results, J. Phys. Appl. Phys. 40 (7) (2007) 1880–1889.
[11] M. Wahl, Time-correlated Single Photon Counting, Technical note, PicoQuant, 2014.
[12] M. Wahl, S. Orthaus-Mueller, Time Tagged Time-Resolved Fluorescence Data Collection in Life Sciences, Technical note, PicoQuant, 2014.
[13] W. Becker, Advanced Time-Correlated Single Photon Counting Techniques, Springer, 2005.
[14] M.L. Chithambo, C. Ankjærgaard, V. Pagonis, Time-resolved luminescence from quartz: an overview of contemporary developments and applications, Phys. B Condens. Matter 481 (2016) 8–18.
[15] T. Lapp, M. Jain, C. Ankjærgaard, L. Pirtzel, Development of pulsed stimulation and photon timer attachments to the Risø TL/OSL reader, Radiat. Meas. 44 (5) (2009) 571–575.
[16] J.S. Nyemann, P. Balling, E.G. Yukihara, Recombination lifetimes of LiF:Mg,Cu,P for pulsed optically stimulated luminescence, J. Lumin. 234 (117924) (2021).
[17] L. Bøtter-Jensen, S.W.S. McKeever, A.G. Wintle, Optically Stimulated Luminescence Dosimetry, Elsevier, 2003.
[18] M.L. Chithambo, A.N. Nyirenda, A.A. Finch, N.S. Rawat, Time-resolved optically stimulated luminescence and spectral emission features of $\alpha$-$Al_2O_3$:C, Phys. B Condens. Matter 473 (2015) 62–71.

[19] W.M. Yen, S. Shionoya, H. Yamamoto, Phosphor Handbook, CRC Press, 2007.
[20] L.D. Carlos, R.A.S. Ferreira, V. de Zea Bermudez, B. Julián-López, P. Escribano, Progress on lanthanide-based organic–inorganic hybrid phosphors, Chem. Soc. Rev. 40 (2011) 536–549.
[21] S. SeethaLekshmi, A. Ramya, M. Reddy, S. Varughese, Lanthanide complex-derived white-light emitting solids: a survey on design strategies, J. Photochem. Photobiol. C Photochem. Rev. 33 (2017) 109–131.
[22] K. Kuriki, Y. Koike, Y. Okamoto, Plastic optical fiber lasers and amplifiers containing lanthanide complexes, Chem. Rev. 102 (6) (2002) 2347–2356.
[23] S.K. Gupta, J.P. Zuniga, M. Abdou, M.P. Thomas, M. De Alwis Goonatilleke, B. S. Guiton, Y. Mao, Lanthanide-doped lanthanum hafnate nanoparticles as multicolor phosphors for warm white lighting and scintillators, Chem. Eng. J. 379 (122314) (2020).
[24] E. Yukihara, E. Milliken, L. Oliveira, V. Orante-Barrón, L. Jacobsohn, M. Blair, Systematic development of new thermoluminescence and optically stimulated luminescence materials, J. Lumin. 133 (2013) 203–210.
[25] L. Oliveira, E. Yukihara, O. Baffa, Lanthanide-doped MgO: a case study on how to design new phosphors for dosimetry with tailored luminescent properties, J. Lumin. 209 (2019) 21–30.
[26] L. Yuan, Y. Jin, Y. Su, H. Wu, Y. Hu, S. Yang, Optically stimulated luminescence phosphors: principles, applications, and prospects, Laser Photon. Rev. 14 (2000123) (2020).
[27] V. Altunal, V. Guckan, A. Ozdemir, A. Ekicibil, F. Karadag, I. Yegingil, Y. Zydhachevskyy, Z. Yegingil, A systematic study on luminescence characterization of lanthanide-doped BeO ceramic dosimeters, J. Alloys Compd. 876 (160105) (2021).
[28] P. Dorenbos, A.J.J. Bos, Lanthanide level location and related thermoluminescence phenomena, Radiat. Meas. 43 (2) (2008) 139–145.
[29] M.W. Swinney, J.W. McClory, J.C. Petrosky, S. Yang, A.T. Brant, V.T. Adamiv, Y. V. Burak, P.A. Dowben, L.E. Halliburton, Identification of electron and hole traps in lithium tetraborate ($Li_2B_4O_7$) crystals: oxygen vacancies and lithium vacancies, J. Appl. Phys. 107 (113715) (2010).
[30] E. Pekpak, A. Yilmaz, G. Ozbayoglu, An overview on preparation and TL characterization of lithium borates for dosimetric use, Open Miner. Process. J. 3 (2010) 14–24.
[31] O. Annalakshmi, M. Jose, U. Madhusoodanan, J. Sridevi, B. Venkatraman, G. Amarendra, A. Mandal, Thermoluminescence mechanism in rare-earth-doped magnesium tetra borate phosphors, Radiat. Eff. Defect Solid 169 (7) (2014) 636–645.
[32] S. Watanabe, E.F. Chinaglia, M.L.F. Nascimento, M. Matsuoka, Thermoluminescence mechanism in $Li_2B_4O_7$:Cu, Radiat. Protect. Dosim. 65 (1–4) (1996) 79–82.
[33] A.V. Porotnikov, I. Ogorodnikov, S.V. Kudyakov, A.V. Kruzhalov, S.L. Votyakov, EPR of hole centers in nonlinear $LiBO_3$ crystals, Phys. Solid State 39 (8) (1997) 1224–1227.
[34] I. Ogorodnikov, L.I. Isaenko, A. Kruzhalov, A. Porotnikov, Thermally stimulated luminescence and lattice defects in crystals of alkali metal borate $LiB_3O_5$ (LBO), Radiat. Meas. 33 (5) (2001) 577–581.
[35] L.C. Oliveira, O. Baffa, Optically and thermally stimulated luminescence of $CaB_6O_{10}$:Ce,LiCl: basic properties, J. Lumin. 188 (2017) 180–187.
[36] R.D. Shannon, Revised effective ionic radii and systematic studies of interatomic distances in halides and chalcogenides, Acta Crystallogr. A 32 (5) (1976) 751–767.
[37] L.V. França, O. Baffa, Boosted UV emission on the optically and thermally stimulated luminescence of $CaB_6O_{10}$:Gd,Ag phosphors excited by X-rays, Appl. Mater. Today 21 (100829) (2020).
[38] M. Eichelbaum, K. Rademann, Plasmonic enhancement or energy transfer? On the luminescence of gold-, silver-, and lanthanide-doped silicate glasses and its potential for light-emitting devices, Adv. Funct. Mater. 19 (13) (2009) 2045–2052.
[39] J.A. Jimenez, Enhanced UV emission of $Gd^{3+}$ in glass by $Ag^{+}$ co-doping, Mater. Lett. 159 (2015) 193–196.
[40] BIPM, IEC, IFCC, ILAC, ISO, IUPAC, IUPAP, OIML, JCGM 100:2008 - Evaluation of Measurement Data - Guide to the Expression of Uncertainty in Measurement, 2008.
[41] W.T. Carnall, P.R. Fields, K. Rajnak, Electronic energy levels of the trivalent lanthanide aquo ions. II. $Gd^{3+}$, J. Chem. Phys. 49 (10) (1968) 4443–4446.
[42] A. Meijerink, M.M.E. van Heek, G. Blasse, Luminescence of $Ag^{+}$ in crystalline and glassy $SrB_4O_7$, J. Phys. Chem. Solid. 54 (8) (1993) 901–906.
[43] R. Reisfeld, E. Greenberg, R. Velapoldi, B. Barnett, Luminescence quantum efficiency of Gd and Tb in borate glasses and the mechanism of energy transfer between them, J. Chem. Phys. 56 (4) (1972) 1698–1705.
[44] A. Kumar, D.K. Rai, S.B. Rai, The effect of modifiers on the fluorescence and life-time of $Gd^{3+}$ ions doped in borate glasses, Spectrochim. Acta Mol. Biomol. Spectrosc. 57 (13) (2001) 2587–2591.
[45] B. Zhang, S. Ying, L. Han, J. Zhang, B. Chen, Color-tunable phosphor of $Sr_3YNa(PO_4)_3F:Tb^{3+}$ via interionic cross-relaxation energy transfer, RSC Adv. 8 (2018) 25378–25386.
[46] J.F.M. dos Santos, I.A.A. Terra, N.G.C. Astrath, F.B. Guimarães, M.L. Baesso, L.A. O. Nunes, T. Catunda, Mechanisms of optical losses in the $^5D_4$ and $^5D_3$ levels in $Tb^{3+}$ doped low silica calcium aluminosilicate glasses, J. Appl. Phys. 117 (053102) (2015).
[47] V. Bachmann, C. Ronda, A. Meijerink, Temperature quenching of yellow $Ce^{3+}$ luminescence in YAG:Ce, J. Chem. Phys. 21 (2009) 2077–2084.
[48] S.K. Sharma, Y.-C. Lin, I. Carrasco, T. Tingberg, M. Bettinelli, M. Karlsson, Weak thermal quenching of the luminescence in the $Ca_3Sc_2Si_3O_{12}:Ce^{3+}$ garnet phosphor, J. Mater. Chem. C 6 (2018) 8923–8933.
[49] N. Shrestha, D. Vandenbroucke, P. Leblans, E. Yukihara, Feasibility studies on the use of $MgB_4O_7$:Ce,Li-based films in 2D optically stimulated luminescence dosimetry, Phys. Open 5 (2020) 100037.
[50] C. Pedrini, Spectroscopic investigation of isolated silver ions in lithium chloride single crystal, J. Phys. Chem. Solid. 41 (6) (1980) 653–657.
[51] C. Pedrini, H. Chermette, F. Gaume-Mahn, Luminescence properties and electronic structure of $Cu^{+}$ and $Ag^{+}$ impurity centers occupying ideal lattice sites in alkali halides, J. Lumin. 24–25 (1981) 213–216.
[52] J.A. Jimenez, S. Lysenko, G. Zhang, H. Liu, Optical properties of silver-doped aluminophosphate glasses, J. Mater. Sci. 42 (2007) 1856–1863.